Crystallization-Induced Orientation for Microstructures of Poly(L-lactide)-*b*-poly(ϵ-caprolactone) Diblock Copolymers

Rong-Ming Ho*

Department of Chemical Engineering, National Tsing Hua University, Hsinchu 30013, Taiwan, R.O.C., and Industrial Technology Research Institute, Union Chemical Laboratories, Hsinchu 30013, Taiwan, R.O.C.

Ping-Yen Hsieh and Wen-Hsien Tseng

Department of Chemical Engineering, National Chung-Hsing University, Taichung 40227, Taiwan, R.O.C.

Chu-Chien Lin and Bor-Han Huang

Department of Chemistry, National Chung-Hsing University, Taichung 40227, Taiwan, R.O.C.

Bernard Lotz

Institut Charles Sadron (CNRS-ULP), 6, rue Boussingault, F-67083 Strasbourg, France

Received June 10, 2003; Revised Manuscript Received September 24, 2003

ABSTRACT: The formation of large-sized, well-oriented microdomains of poly(L-lactide)-*b*-poly(ϵ-caprolactone) (PLLA−PCL) was successfully achieved by using different crystalline substrates including benzoic acid (BA) and hexamethylbenzene (HMB), whereas spherulitic crystalline texture was obtained on amorphous substrates. Crystallization-induced orientation of PLLA−PCL microstructures is attributed to directional crystallization of eutectic type between crystalline PLLA and substrate, regardless of microphase separation. Surprisingly, a flat-on crystalline morphology (i.e., with the chain axis normal to the substrate) was obtained, as evidenced by single-crystal-like [001] zonal electron diffraction (ED). By contrast, an edge-on crystalline morphology (i.e., with the chain axis parallel to the substrate) was observed for PLLA homopolymer under the same condition. The crystallographic organization of PLLA−PCL microdomains as observed by transmission electron microscopy, ED, and scanning probe microscopy suggests that the growth direction of PLLA crystals is along the *a*-axis direction, which suggests that the growth direction of PLLA crystals is along the *a*-axis direction that corresponds well with the preferential growth direction (i.e., *b*-axis direction) of BA or HMB crystals. As a result, the phase-separated lamellar morphology consists of an alternation of a flat-on layer of PLLA lamellae and of an amorphous layer of PLLA and PCL components.

Introduction

The self-assembly of block copolymers driven by immiscibility between constituted blocks generates nanoscale microstructures that appear promising in the applications of nanotechnologies,[1−4] particularly the formation of a nanopatterned template for nanodevice applications. Aliphatic polyesters represent an important family of biodegradable materials.[5−8] Increasing attention has been focused on hydrolytically unstable lactone or lactide polymers owing to their biodegradable characters. Block copolymers containing polyesters such as poly(ϵ-caprolactone) (PCL) and poly(L-lactide) (PLLA) are a new family for the preparation of nanopatterned templates because polyester blocks can be selectively degraded by hydrolysis treatment[4,9,10] or enzymatic degradation,[11,12] thus forming regularly patterned topography in thin-film samples.

For such polymers to prove useful in nanotechnologies, well-oriented periodic arrays must be made over a large area. Different approaches to control the orientation of phase-separated microstructures have been used: shear fields,[13−17] electric fields,[18,19] magnetic fields,[20,21] patterned substrates,[22−24] and temperature gradients.[25,26] Recently, a novel way to create large-sized, well-oriented microdomains of block copolymers has been proposed by Thomas and co-workers.[27,28] Epitaxial crystallization was used to control both molecular chain and microstructure orientations for crystallizable block copolymers, in which the orientations were induced by crystallization from a homogeneous melt. As initially proposed by Wittmann and Lotz, epitaxy-induced orientation of homopolymers stems from structural similarities and one- or two-dimensional lattice matching between crystalline polymer and underlying substrate.[29−31] For block copolymers, well-oriented microdomains over hundreds of μm^2 were obtained by epitaxial crystallization of crystallizable block onto crystalline substrate. Edge-on crystalline morphology (i.e., with the chain axis parallel to the substrate) was observed for crystallization-induced microdomains of crystallizable block copolymers.[27,32]

Here, our aim is to examine the mechanism of crystallization-induced orientation for the biodegradable diblock copolymers, PLLA−PCL, of which both blocks are crystallizable. Large-sized, well-oriented microdomains of PLLA−PCL were induced by different crystalline substrates. Contrary to previous findings, flat-on crystalline lamellae (i.e., with the chain axis normal to the substrate) of PLLA blocks were obtained on the top of crystalline substrate. A hypothetical phase diagram of eutectic behavior for a solvent−crystalline

* To whom all correspondence should be addressed. Tel 886-3-5738349; Fax 886-4-5715408; e-mail rmho@mx.nthu.edu.tw.

10.1021/ma0347868 CCC: $25.00
Published on Web 10/30/2003

polymer system, as proposed by previous works,[32] was used to interpret the mechanism of crystallization-induced orientation for PLLA−PCL block copolymers.

Experimental Section

For the synthesis of PLLA−PCL diblock copolymer, ring-opening polymerization was used to carry out sequential living polymerization of PCL and PLLA blocks. The ring-opening polymerization was catalyzed and controlled by a novel aluminum alkoxide complex synthesized in our laboratory.[33] Size exclusion chromatography (SEC) indicated that the number-average molecular weight, M_n, is ca. 33 900 g/mol and a polydispersity index is ca. 1.2. The molecular weight of PLLA−PCL determined by ^{1}H NMR is 23 600 g/mol; PLLA and PCL blocks are 17 400 and 6200 g/mol, respectively.[33] On the basis of NMR results, the volume fraction of PCL block was calculated as 0.28 while the densities of PLLA and PCL are 1.18[34] and 1.08 g/cm^3,[35] respectively. The molecular weight and polydispersity index of PLLA homopolymer used are ca. 21 200 g/mol and 1.05, respectively.

DSC experiments were carried out in a Perkin-Elmer DSC 7 for the measurements of thermal behavior for PLLA−PCL, benzoic acid (BA), and hexamethylbenzene (HMB). PLLA blocks melt at around 152 °C. The maximum crystallization rate of PLLA blocks under 150 °C/min cooling rate is at 82 °C. T_g's of PLLA and PCL are approximately 50 and −60 °C, respectively. Melting temperatures of BA and HMB are 123 and 168 °C, respectively.

Epitaxial crystallization of PLLA−PCL was performed following the procedure described by De Rosa and co-workers[27,32] as well as Cartier and co-workers.[36] PLLA−PCL thin films were first formed on carbon-coated microscope glass slides by spin-coating from dichloroethane (CH_2Cl_2) solution (0.5 wt % of PLLA−PCL) at room temperature. The thickness of the thin films is 20−30 nm as determined by scanning probe microscopy (SPM). The method for the thickness measurements by SPM is similar to the procedures described by Möller and co-workers.[37] Powders of crystalline organic solvent (i.e., BA or HMB) were spread over onto the spin-coated samples and then covered by previous thin-film sample. The assembly with block copolymer sandwiched by the crystalline powders of BA or HMB and carbon-coated slide was heated to 150 and 170 °C in the presence of BA (T_m = 123 °C) and HMB (T_m = 168 °C), respectively; a clear solution was formed within glass slides. The solution was then cooled (at a rate of 150 °C/min) to preset crystallization temperatures (T_c). The supercooling first induced rapid directional crystallization of BA or HMB at T_c = 80 °C, followed by crystallization of PLLA−PCL onto crystalline BA or HMB. After crystallization, crystalline BA and HMB were dissolved in ethyl alcohol at 50 °C and in acetone at room temperature, respectively. The composite polymer-carbon film was floated off the glass onto water and mounted on copper grids. Transmission electron microscopy in bright field and corresponding selected area diffraction were performed with JEOL TEM-1200x transmission electron microscopy as described in our previous paper.[38] Staining was accomplished by exposing the samples to the vapor of a 4% aqueous RuO_4 solution for 2 h. PLLA−PCL thin films prepared by simple spin-coating on carbon-coated glass slides were also analyzed for comparison. Bright field TEM images and SPM images by tapping mode were obtained from these thin-film samples. A Seiko SPA-400 AFM with a SEIKO SPI-3800N probe station was employed at room temperature in this work. A rectangle-shaped silicon tip was applied in dynamic force mode (DFM) experiments using a type of SI-DF40 with a spring force contact of 41 N m^{-1} and scan rate of 1.5 Hz.

Results and Discussion

Phase-Separated and Crystallized Morphology. To study the phase behavior of PLLA−PCL thin films, thin-film samples on carbon-coated glass slide after quench from melt were examined by using TEM and SPM. The thickness of thin films was approximately 20−30 nm as determined by SPM. No significant morphological texture for the thin films after RuO_4 staining was observed by TEM due to the lack of contrast between amorphous PCL and PLLA. By contrast, the phase image of SPM observation under dynamic force mode exhibits disordered phase-separated texture of which dark PCL matrix indicates less phase delay than bright PLLA dispersed domains (Figure 1). The morphological observation demonstrates that quenched PLLA−PCL thin film exhibits disordered texture at room temperature. The observed morphology is consistent with the prediction of phase behavior on the basis of mean-field theory calculation. A rough estimate of the Flory interaction parameter χ can be obtained from the equation $\chi = \mathrm{Vu}/RT(\delta_{PCL} - \delta_{PLLA})^2$, where the arbitrary reference volume Vu is conveniently selected as 100 cm^3/mol, and the solubility parameters are approximately 9.39[39] and 9.79[40] (cal/cm^3)$^{0.5}$ for PCL and PLLA, respectively. At a crystallization temperature window of PLLA ranging from 180 to 50 °C, the χN values are approximately 2.87−4.03. Theoretically, the χN value is too low (i.e., much lower than 10.5) for the block copolymer to segregate and to self-assemble as ordered structure at the temperatures; despite the crudeness of using solubility parameters and ignoring entropic contribution to estimate the χ value, we conclude that the polymeric system should be a disordered phase at the studied temperature range.

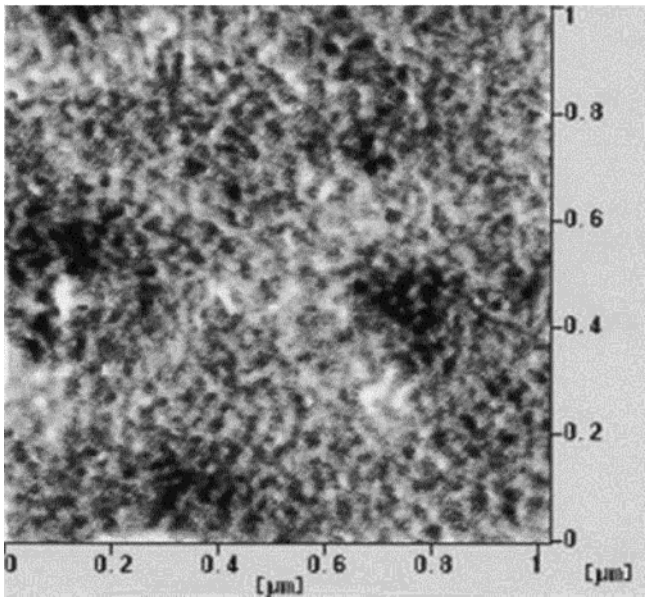

Figure 1. Tapping-mode SPM phase image of spin-coated PLLA−PCL thin film quenched from 170 °C. The phase delay scale is 4.3°.

To observe crystallized morphology for PLLA−PCL at different T_c, thin films on carbon-coated glass slide were crystallized from melt. The crystallized thin films were then shadowed Pt and coated with carbon again. After shadowing, the thin films were stripped and floated onto the surface and then recovered using copper grids. Figure 2a shows TEM micrograph of PLLA−PCL isothermally crystallized at 80 °C from 170 °C. Branching crystalline lamellae can be clearly recognized. Similar crystalline morphology was obtained for PLLA−PCL isothermally crystallized in the crystallization window of PLLA (i.e., $T_{m,PLLA}$ (∼160 °C) > T_c > $T_{g,PLLA}$ (∼45 °C)). By contrast, PCL crystallization occurs while PLLA−PCL samples isothermally crystallized at lower temperature (i.e., $T_{m,PCL}$ (∼50 °C) > T_c > $T_{g,PCL}$ (∼−60

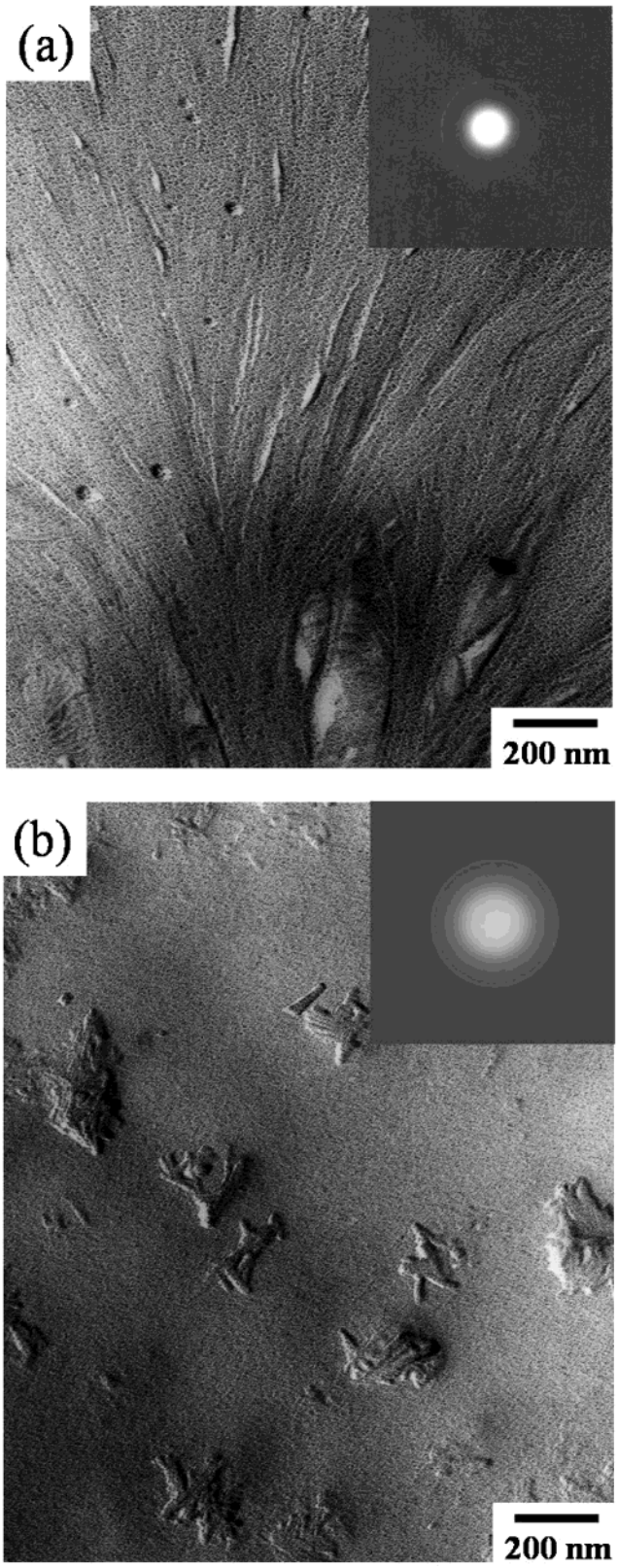

Figure 2. TEM micrographs of spin-coated PLLA-PCL thin films (a) crystallized at 80 °C from melt (170 °C) and (b) crystallized at ambient temperature from melt (170 °C) after shadowing. The inset ED patterns were obtained from the central area of the micrograph and shown in correct orientation. The diffractions in (a) and (b) result from PLLA and PCL crystallites, respectively.

°C)) from melt. Tiny crystalline texture was formed as an example illustrated in Figure 2b. As a result, morphologies of PLLA−PCL thin films on carbon-coated

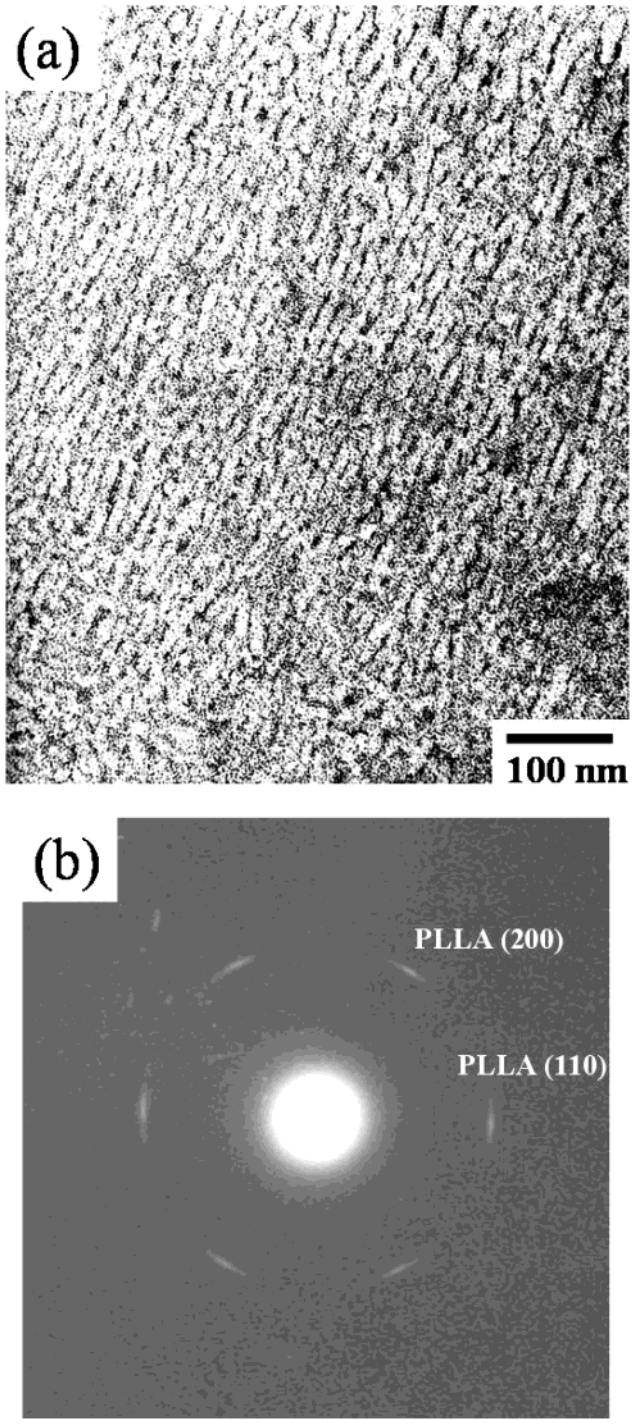

Figure 3. TEM micrograph of spin-coated PLLA−PCL thin film (a) directionally crystallized at 80 °C on top of BA crystals after staining. (b) The ED pattern was obtained from the central area of the micrograph and shown in correct orientation.

substrate exhibit random orientation for phase-separated textures whether they are crystallized or at amorphous state.

Epitaxy-Induced Morphology. To control the orientation of PLLA−PCL microdomains, PLLA−PCL thin films were epitaxially crystallized onto crystalline BA substrate. As observed by PLM, BA first crystallized as single-crystal-like crystals elongated in the crystallographic *b* direction with large (001) surface. Following BA crystallization, epitaxy-induced PLLA−PCL crystallization gave rise to the formation of large-scale, well-oriented microdomains with lamellar texture as shown

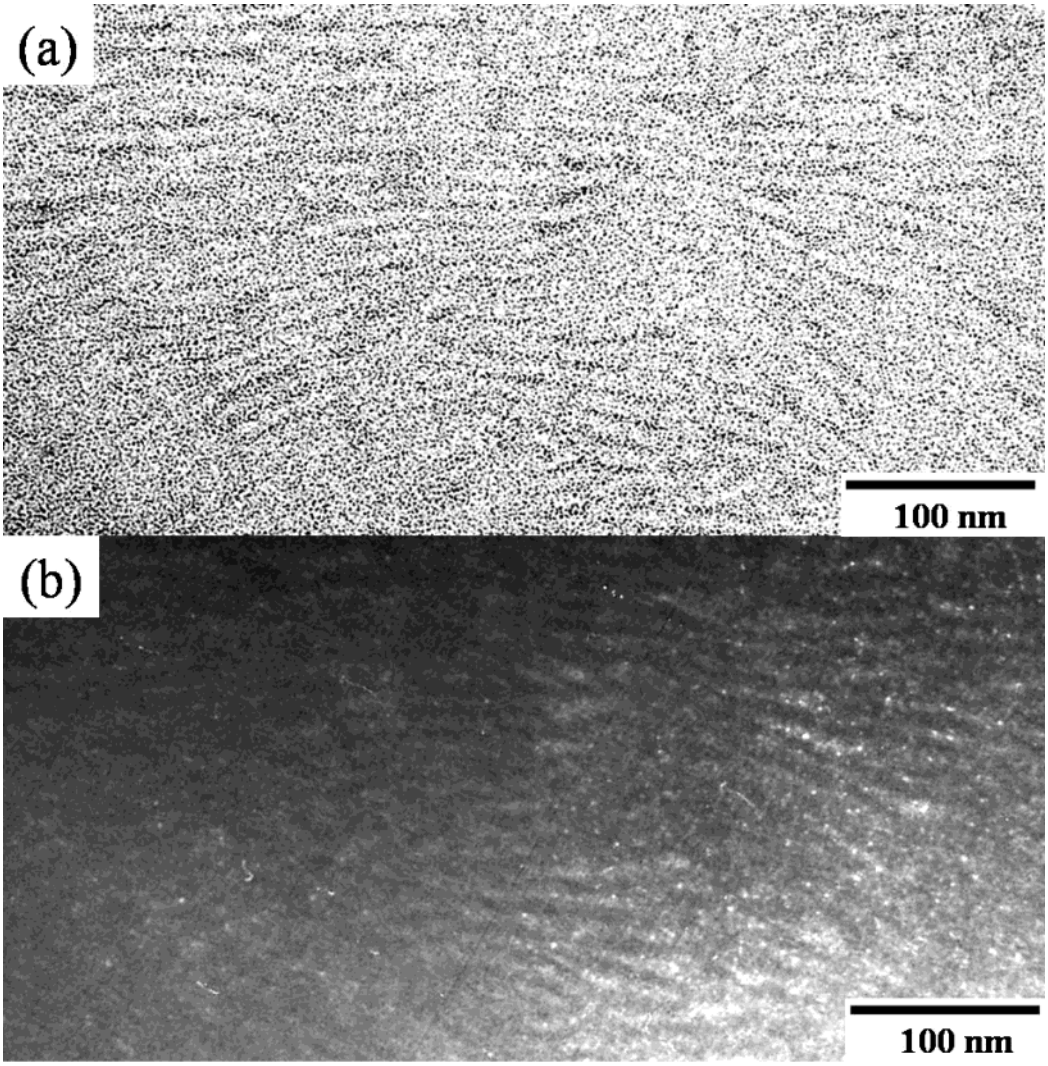

Figure 4. TEM (a) bright field and (b) dark field micrograph of spin-coated PLLA−PCL thin film directionally crystallized at 80 °C on top of BA crystals after staining.

in Figure 3a. The size of the oriented microdomains can be as large as thousands of μm^2. Selected area electron diffraction pattern of epitaxy-induced PLLA−PCL microdomains is shown in Figure 3b. A single-crystal-like electron diffraction pattern can be obtained. On the basis of the α form of PLLA crystals with unit cell of $a = 1.07$ nm, $b = 0.595$ nm, $c = 2.78$ nm, and $\alpha = \beta = \gamma = 90°$,[36,41] the corresponding primary reflections were identified as (200) and (110) for pseudo-orthorhombic crystalline structure; it indicates a [001] zonal electron diffraction. As a result, the epitaxy-induced PLLA crystallization in PLLA−PCL not only generated large-scale uniform orientation for the lamellar microstructure but also exhibited unique molecular disposition in that chain molecules in PLLA crystalline phase are normal to epitaxial substrate (i.e., a flat-on PLLA crystalline lamellae). There is always the possibility that image and diffraction patterns have come from different regions in bright field. Dark field microscopy would have left no doubt for the identification of flat-on morphology. To further confirm the suggested morphology, dark field image from (110) or (200) reflections was obtained as shown in Figure 4. The dark field results confirm that the [00*l*] zonal diffraction is indeed contributed by oriented crystalline PLLA microdomains.

Consequently, the results indicate the existence of lattice matching between PLLA and BA crystals since the crystalline fold surface of PLLA is in contact with the crystalline (001) plane of BA for epitaxial crystallization. On the assumption of regularly adjacent reentry model for folding surface, this lattice matching can be well described in terms of matching the PLLA interchain distances of *a*-axis and *b*-axis periodicities ($a = 1.07$ nm and $b = 0.595$ nm for the α form of PLLA) with the *b*-axis and *a*-axis periodicities of BA unit cell ($b = 0.51$ nm and $a = 0.552$ nm[42,43]), as illustrated in Figure 5. The dimension of PLLA *a*-axis is approximately 2 times that of BA *b*-axis, and the dimension of PLLA *b*-axis is approximately equal to that of BA *a*-axis; the corresponding mismatchings are 4% and 7%, respectively. The inference of lattice matching is further confirmed by observed crystallographic geometry of PLLA crystals with respect to the molecular disposition of induced microdomains. As shown in Figure 3, the morphology and ED pattern indicate that the molecular chain axis of PLLA crystallites is perpendicular to BA substrate and phase-separated lamellar normal. The growth direction of PLLA crystals is the *a*-axis direction on the assumption that the growth direction of epitaxy-induced crystals corresponds to the preferential growth direction (i.e., *b*-axis direction) of BA crystals. However, it is noted that the growth plane of homopolymer PLLA for solution-growth single crystals has been identified as (110) instead of (100).[44] This indicates that growth

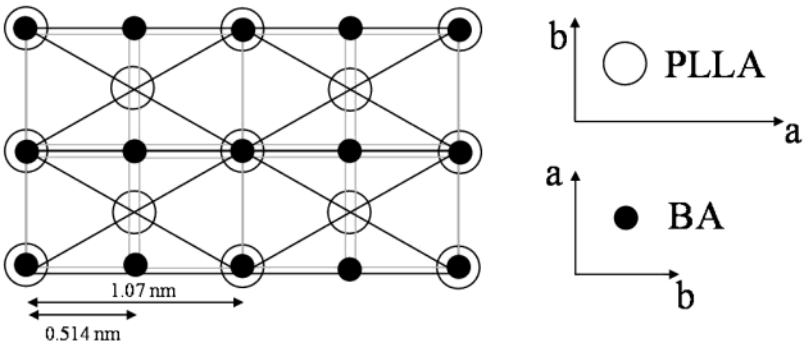

Figure 5. Illustration of lattice matching between the (001) plane of crystalline BA and the (001) plane of crystalline PLLA.

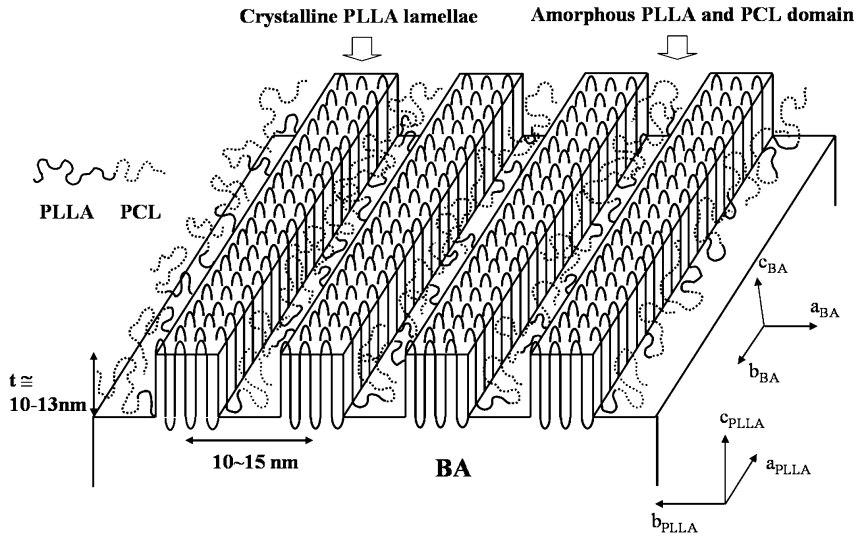

Figure 6. Schematic representation of flat-on PLLA crystalline morphology in PLLA−PCL epitaxially crystallized onto BA.

Table 1. Comparisons of Crystallized Morphology of PLLA Homopolymer and PLLA−PCL Copolymer from Various Substrates

		substrate		
thin film		amorphous surface	BA	HMB
PLLA homopolymer	molecular chains	random	random	edge-on
	phase-separated microdomains	no preferred orientation	no preferred orientation	large-scale orientation
PLLA−PCL	molecular chains	random	flat-on	flat-on
	phase-separated microdomains	no preferred orientation	large-scale orientation	large-scale orientation

mechanism for epitaxy-induced crystallization of PLLA blocks might be different to that of homopolymer PLLA. It is also noted that the crystallinity of PCL generated at room temperature is trivial, thus leading to the absence of diffraction intensity under TEM. Similar to the spatial confinement effect on crystallization, the microdomains generated by PLLA crystallization indeed inhibits PCL crystallization. However, increasing the PCL content of block copolymers will relieve the confinement effect and result in the crystallization of PCL blocks within crystalline PLLA microdomains. Detailed studies for the confinement effect of PLLA crystals on PCL crystallization are still under investigation and will be reported in another paper.

Molecular Disposition. The averaged lateral distance between flat-on PLLA crystals is 10−15 nm, and the thickness of epitaxy-induced layer is around 10−13 nm as determined by TEM and SPM. As reported by Miyata and co-workers, the lamellar thickness of solution-grown single crystal for homopolymer PLLA is 10−11 nm as determined by SPM.[44] For PLLA−PCL, the lamellar thickness of PLLA crystalline in PLLA−PCL melt-crystallized from bulk is 9−10 nm as determined by SAXS.[45] Although the crystalline lamellar thickness is strongly dependent upon crystallization conditions, particularly the crystallization temperature, we simply compare these results with the thickness of epitaxy-induced layer. On the assumption of 10 nm lamellar thickness, we suggest that epitaxy-induced microdomains of PLLA−PCL possess phase-separated lamellar morphology with an alternation of flat-on single layer of PLLA lamellae and of amorphous layer of PLLA and PCL components. Figure 6 shows this schematic model. The formation of phase-separated lamellar morphology was driven by the crystallization of PLLA blocks so as to form large-scale orientation because of epitaxy-induced origin. By contrast, crystallization-induced neat PLLA crystals by HMB exhibited typical edge-on morphology in this study (Table 1). Cartier and co-workers have observed similar results.[36] In general, epitaxy-induced crystallization either for homopolymers or for block copolymers generates only edge-on crystal morphology. For instance, the chain axis of crystalline PE in polyethylene−poly(ethylene-*alt*-propylene)−polyethylene (PE−PEP−PE) is parallel to epitaxial substrate and the normal of microphase-separated lamellae.[27]

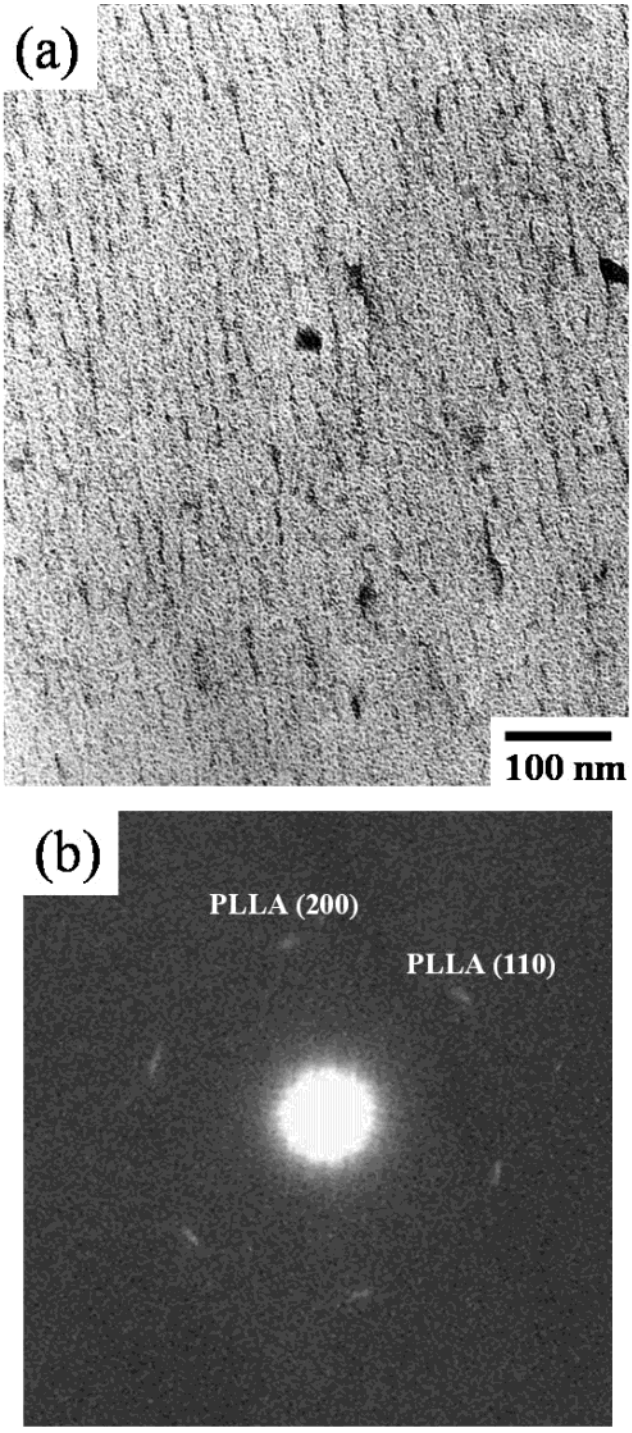

Figure 7. TEM micrographs of spin-coated PLLA-PCL thin film (a) directionally crystallized at 80 °C on top of HMB crystals after staining. (b) The ED pattern was obtained from the central area of the micrograph and shown in correct orientation.

Further investigation is necessary to clarify the discrepancies with respect to molecular dispositions of crystallization-induced PLLA crystallites. Nevertheless, flat-on PLLA crystalline morphology for epitaxy-induced PLLA-PCL on BA substrate is formed rather than the more usual and expected edge-on crystalline morphology.

Crystallization-Induced Morphology. By contrast, another substrate, namely the HMB just mentioned, was chosen to carry out similar experiments. Large-sized, oriented microdomains induced by HMB were also

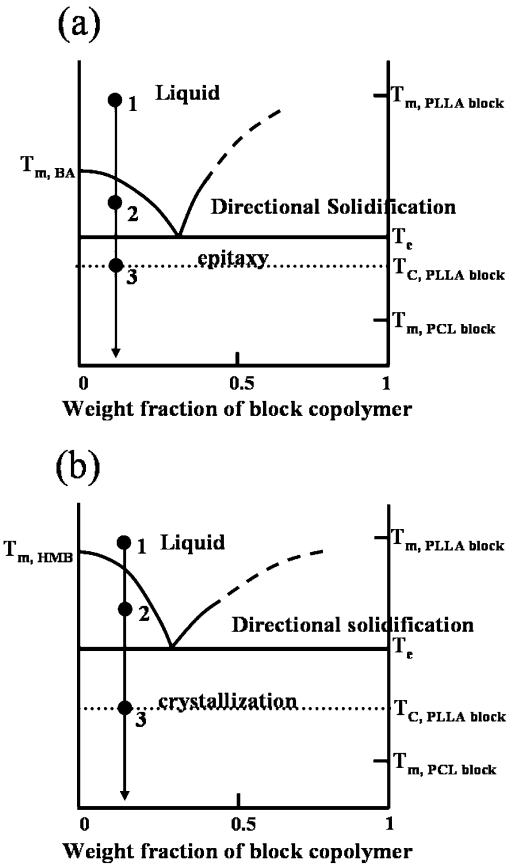

Figure 8. Hypothetical phase diagram of solvent−polymer system.

obtained, as shown in Figure 7a. Again, the [001] zonal ED pattern (Figure 7b, similar to Figure 2b) indicates that the chain axis is perpendicular to substrate surface. However, lattice matching between the *ab* plane of PLLA and the *ab* plane of HMB does not exist. The unit cell parameters of HMB were determined as $a = 0.892$ nm, $b = 0.886$ nm, $c = 0.53$ nm, $\alpha = 44.3°$, $\beta = 116.4°$, and $\gamma = 119.3°$.[46] The observations raise a question with respect to the origin of large-scale orientation and their corresponding molecular dispositions. Is lattice matching critical for the formation of large-scale orientation of microdomains induced by crystalline substrate?

Different substrates have been used to carry out crystallization process for PLLA homopolymer and PLLA−PCL as summarized in Table 1. Obviously, the induction of orientation is originated by the crystallization event of PLLA components onto single-crystal-like crystalline substrate. By contrast, spherulitic crystalline texture was obtained from amorphous substrate. Different interpretations such as the mixing−demixing effect, interfacial tension effect, and lattice matching origin have been given to explain the initiation of crystallization-induced orientation for block copolymers. As observed, the criterion of lattice matching is not necessary for crystallization-induced orientation. Park and co-workers have made similar remarks for the induction of PS−PMMA orientation by using BA since the PS−PMMA is noncrystallizable.[28] As a result, large-scale orientation might be promoted by suitable crystalline substrate, but the criterion of lattice matching is not needy to fulfill. We speculate that the eutectic growth of crystalline substrate not only excludes out the block copolymer chains but also creates a specific

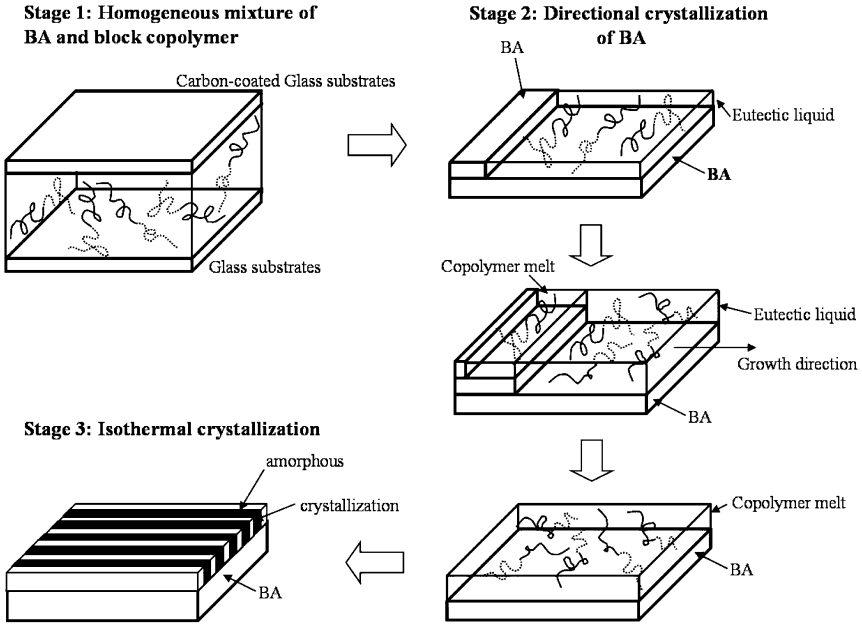

Figure 9. Illustration of morphology evolution for crystallization-induced orientation of PLLA−PCL.

crystalline surface to induce the orientation of following crystallization for block copolymers.

Morphological Evolution. The mechanism for crystallization-induced orientation of block copolymers has been clearly described by De Rosa and co-workers in term of the directional eutectic solidification concept.[32] As described, the overall phase transformation has been divided into three stages using a hypothetical solvent−polymer phase diagram (Figure 4 in ref 34). An important feature of the phase diagram is the presence of a eutectic due to the intersection of melting-point depression liquidus curve of BA with microphase-separation-transition depression liquidus curve of block copolymer. By contrast, the order−disorder transition temperature (T_{ODT}) of PLLA−PCL is below the crystallization window for the PLLA component. In other words, the formation of ordered, microphase-separated microdomains does not occur before crystallization. The sequences of crystallization events for crystalline solvent−PLLA−PCL are slightly different than the proposed mechanism by de Rosa and co-workers. A modified hypothetical solvent−polymer phase diagram is thus proposed as shown in Figure 8, and the corresponding morphological evolution is depicted (Figure 9). Here, the eutectic point is intrinsically the intersection of melting-point depression liquidus curve of BA with equilibrium-melting-point depression liquidus curve of PLLA blocks. At high temperature, the solvent−polymer system begins as a homogeneous liquid (stage 1). Crystallization of crystalline substrate carries out by decreasing temperature below melting-point depression liquidus curve. Further decreasing temperature, the growth of crystalline substrate leads to the increase of polymer content in remaining solution toward eutectic composition (stage 2). Once the cooling temperature reaches the eutectic temperature, crystallization of PLLA blocks initiates and transforms eutectic liquid into crystalline substrate and solidified PLLA−PCL where PLLA chains crystallize as crystalline lamellae (stage 3) The formation of large-scale, well-ordered phase-separated lamellar microstructure is thus formed after the whole crystallization events for the solvent−polymer system. Complete crystallization of PLLA−PCL results in microphase-separated-like morphology and ordered lamellar morphology with an alternation of flat-on single layer of PLLA lamellae and of amorphous layer of PLLA and PCL components. As a result, the crystallization-induced orientation is attributed to the directional crystallization of PLLA blocks onto single-crystal-like crystalline substrate.

Conclusion

Unique self-assembly morphology of PLLA−PCL, large-sized, well-oriented phase-separated microdomains with flat-on crystalline morphology was obtained. The formation of nanopatterned microdomains is suggested to be in accordance with the effect of crystallization-induced orientation. Besides the utilization of BA crystalline substrate, the formation of large size microdomains can also be obtained by using HMB crystalline substrate. Unlike BA, lattice matching between crystalline PLLA and HMB does not exist. As a result, lattice matching does not seem to be a critical issue for the induction of orientation for PLLA−PCL. Here, we present a possible way to prepare the large-scale orientation of microdomains for biodegradable PLLA−PCL diblock copolymer.

Acknowledgment. The financial support of the National Science Council (Grant NSC-90-2216-E-005-011) is acknowledged. The authors thank Dr. S. Z. D. Cheng of Institute of Polymer Science of University of Akron for helpful discussions. R.M.H. also thanks Ms. P.-C. Chao of Regional Instruments Center at NCHU and Dr. S.-H. Chen at NSYSU for her help in TEM and ED experiments.

References and Notes

(1) Mansky, P.; Chaikin, P. M.; Thomas, E. L. *J. Mater. Sci.* **1995**, *30*, 1987.
(2) Park, M.; Harrison, C.; Chaikin, P. M.; Register, R. A.; Adamson, D. H. *Science* **1997**, *276*, 1401.
(3) Huang, E.; Rockford, L.; Russell, T. P.; Hawker, C. J. *Nature (London)* **1998**, *395*, 757.

(4) Zalusky, A. S.; Olayo-Valles, R.; Taylor, C. J.; Hillmyer, M. A. *J. Am. Chem. Soc.* **2001**, *123*, 1519.
(5) Ye, W.-P.; Du, F.-S.; Jin, W.-H.; Yuan, Y.; Xu, Y. *React. Funct. Polym.* **1997**, *32*, 161.
(6) Leach, K. J.; Mathiowitz, E. *Biomaterials* **1998**, *19*, 1973.
(7) Li, S.; McCarthy, S. P. *Biomaterials* **1999**, *20*, 35.
(8) Lu, L.; Peter, S. J.; Lyman, M. D.; Lin, H.; Leite, S. M.; Tamada, J. A.; Vacanti, J. P.; Langer, R.; Mikos. A. G. *Biomaterials* **2000**, *21*, 1595.
(9) Li, S. *J. Biomed. Mater. Res., Appl. Biomater.* **1999**, *48*, 142.
(10) Hakkarainen, M.; Karlsson, S.; Albertsson, A.-C. *Polymer* **2000**, *41*, 2331.
(11) Li, S.; McCarthy, S. *Macromolecules* **1999**, *32*, 4454.
(12) Gan, Z.; Yu, D.; Zhong, Z.; Liang, Q.; Jing, X. *Polymer* **1999**, *40*, 2859.
(13) Koppi, K. A.; Tirrell, M.; Bates, F. S.; Almdal, K.; Colby, R. H. *J. Phys. II* **1992**, *2*, 1941.
(14) Koppi, K. A.; Tirrell, M.; Bates, F. S. *Phys. Rev. Lett.* **1993**, *70*, 1449.
(15) Maring, D.; Wiesner, U. *Macromolecules* **1997**, *30*, 660.
(16) Gupta, V. K.; Krishnamoorti, R.; Kornfield, J. A. *Macromolecules* **1996**, *29*, 1359.
(17) Cates, M. E.; Milner, S. T. *Phys. Rev. Lett.* **1989**, *62*, 1856.
(18) Morkved, T. L.; Lu, M.; Urbas, A. M.; Ehrichs, E. E.; Jaeger, H. M.; Mansky, P.; Russell, T. P. *Science* **1996**, *273*, 931.
(19) Mansky, P.; DeRouchey, J.; Russell, T. P.; Mays, J.; Pitsikalis, M.; Morkved, T.; Jaeger, H. *Macromolecules* **1998**, *31*, 4399.
(20) Fujiwara, M.; Chidiwa, T.; Tanimoto, Y. *J. Phys. Chem. B* **2000**, *104*, 8075.
(21) Nawa, M.; Baba, R.; Nakabayashi, S.; Dushkin, C. *Nano Lett.* **2003**, *3*, 293.
(22) Yang, X. M.; Peters, R. D.; Nealey, P. F.; Solak, H. H.; Cerrina, F. *Macromolecules* **2000**, *33*, 9575.
(23) Spatz, J. P.; Eibeck, P.; Mössmer, S.; Möller. M.;Kramarenko, E. Y.; Khalatur, P. G.; Potemkin, I. I.; Khokhlov, A. R.; Winkler, R. G.; Reineker, P. *Macromolecules* **2000**, *33*, 150.
(24) Rockford, L.; Mochrie, S. G. J.; Russell, T. P. *Macromolecules* **2001**, *34*, 1487.
(25) Bodycomb, J.; Funaki, Y.; Kimishima, K.; Hashimoto, T. *Macromolecules* **1999**, *32*, 2075.
(26) Hashimoto, T.; Bodycomb, J.; Funaki, Y.; Kimishima, K. *Macromolecules* **1999**, *32*, 952.
(27) De Rosa, C.; Park, C.; Lotz, B.; Wittmann, J. C.; Fetters, L. J.; Thomas, E. L. *Macromolecules* **2000**, *33*, 4871.
(28) Park, C.; De Rosa, C.; Thomas, E. L. *Macromolecules* **2001**, *34*, 2602.
(29) Wittmann, J. C.; Lotz, B. *J. Polym. Sci., Polym. Phys. Ed.* **1981**, 1837.
(30) Wittmann, J. C.; Lotz, B. *J. Polym. Sci., Polym. Phys. Ed.* **1981**, 1853.
(31) Wittmann, J. C.; Hodge, A. M.; Lotz, B. *J. Polym. Sci., Polym. Phys. Ed.* **1983**, 2495.
(32) De Rosa, C.; Park, C.; Thomas, E. L.; Lotz, B. *Nature (London)* **2000**, *405*, 433.
(33) Liu, Y.-C.; Ko, B.-T.; Lin, C.-C. *Macromolecules* **2001**, *34*, 6196.
(34) Zalusky, A. S.; Olayo-Valles, R.; Wolf, J. H.; Hillmyer, M. A. *J. Am. Chem. Soc.* **2002**, *124*, 12761.
(35) Balsamo, V.; Stadler, R. *Macromolecules* **1999**, *32*, 3994.
(36) Cartier, L.; Okihara, T.; Ikada, Y.; Tsuji, H.; Puiggali, J.; Lotz, B. *Polymer* **2000**, *41*, 8909.
(37) Spatz, J. P.; Sheiko, S.; Möller, M. *Adv. Mater.* **1996**, *8*, 513.
(38) Ho, R.-M.; Lin, C.-P.; Hseih, P.-Y.; Chung, T.-M.; Tsai, H.-Y. *Macromolecules* **2001**, *34*, 6727.
(39) Small, P. A. *Appl. Chem.* **1953**, *3*, 71.
(40) Blumm, E.; Owen, A. J. *Polymer* **1995**, *36*, 4077.
(41) Hoogsten, W.; Postema, A. R.; Pennings, A. J.; ten Brinke, G.; Zugenmaier, P. *Macromolecules* **1990**, *23*, 634.
(42) Sarma, K. R.; Shlichta, P. J.; Wilcox, W. R.; Lefever, R. A. *J. Cryst. Growth* **1997**, *174*, 487.
(43) Holmbäck, X.; Rasmuson, A. C. *J. Cryst. Growth* **1999**, *199*, 780.
(44) Miyata, T.; Masuko, T. *Polymer* **1997**, *38*, 4003.
(45) Kim, J. K.; Park, D. J.; Lee, M. S.; Ihn, K. J. *Polymer* **2001**, *42*, 7429.
(46) Brockway, L. O.; Robertson, J. M. *J. Chem. Soc., Part C* **1939**, 1324.

MA0347868